

FS-MPC Algorithm for Optimized Operation of a Hybrid Active Neutral Point Clamped Converter

Novak, Mateja; Ferreira, Victor; Andresen, Markus; Dragicevic, Tomislav; Blaabjerg, Frede; Liserre, Marco

Published in:
2019 IEEE Energy Conversion Congress and Exposition, ECCE 2019

DOI (link to publication from Publisher):
[10.1109/ECCE.2019.8913306](https://doi.org/10.1109/ECCE.2019.8913306)

Publication date:
2019

Document Version
Accepted author manuscript, peer reviewed version

[Link to publication from Aalborg University](#)

Citation for published version (APA):
Novak, M., Ferreira, V., Andresen, M., Dragicevic, T., Blaabjerg, F., & Liserre, M. (2019). FS-MPC Algorithm for Optimized Operation of a Hybrid Active Neutral Point Clamped Converter. In *2019 IEEE Energy Conversion Congress and Exposition, ECCE 2019* (pp. 1447-1453). Article 8913306 IEEE Press.
<https://doi.org/10.1109/ECCE.2019.8913306>

General rights

Copyright and moral rights for the publications made accessible in the public portal are retained by the authors and/or other copyright owners and it is a condition of accessing publications that users recognise and abide by the legal requirements associated with these rights.

- Users may download and print one copy of any publication from the public portal for the purpose of private study or research.
- You may not further distribute the material or use it for any profit-making activity or commercial gain
- You may freely distribute the URL identifying the publication in the public portal -

Take down policy

If you believe that this document breaches copyright please contact us at vbn@aub.aau.dk providing details, and we will remove access to the work immediately and investigate your claim.

FS-MPC Algorithm for Optimized Operation of a Hybrid Active Neutral Point Clamped Converter

Mateja Novak*, Victor N. Ferreira[†], Markus Andresen[†], Tomislav Dragicevic*,
Frede Blaabjerg* and Marco Liserre[†]

*Department of Energy Technology, Aalborg University, Aalborg, Denmark

[†]Chair of Power Electronics, Kiel University, Kiel, Germany

nov@et.aau.dk, vf@tf.uni-kiel.de, ma@tf.uni-kiel.de, tdr@et.aau.dk, fbl@et.aau.dk, ml@tf.uni-kiel.de

Abstract—The design for reliability has gained a lot of attention in power electronic community in the past few years. The aim is to optimize the design in order to achieve desired reliability goals with minimum margins. However, in most applications, there are stressing conditions, which result in high stress and therefore require higher margins. As an opportunity, adapting the control of the power electronic converters to equally redistribute the stress of the devices can reduce the stressing conditions and also reduce the design margins. This is of great importance for multilevel topologies and in particular the Active Neutral Point Clamped (ANPC) topology. This paper introduces a Finite-Set Model Predictive Control algorithm designed for achieving a balanced device junction temperature in a Hybrid SiC ANPC converter. The inner switches of the converter are replaced by SiC MOSFETs and the control algorithm is designed to utilize the low switching losses of the devices. The obtained experimental results are compared to carrier based benchmark algorithm. It is demonstrated that the temperature difference between the devices is within 1°C and the dc-link voltage deviation is within 0.5V.

Index Terms—Active Neutral Point Clamped converter (ANPC), Finite-set Model Predictive Control (FS-MPC), hybrid power stage, multilevel converter, SiC

I. INTRODUCTION

In 1980s the three level neutral point clamped (NPC) converter was introduced for the medium-voltage large variable speed drives to improve the conversion efficiency [1]. Nowadays, the application has also spread in the low voltage range, particularly for interconnection of renewable energy sources [2]–[4]. It was soon noticed that although the topology has brought many benefits such as lower harmonic distortion of the output voltages/currents, smaller and cheaper filters, the maximum output power was still limited by the unbalanced stress distribution of the power components [5], [6]. Efforts have been made to solve the problem by sizing the components for the expected stress [7]. However the problem was still not solved as a different operating point of the converter presented different temperature distributions. For low amplitude modulation indexes the inner devices are more stressed due to increased usage of the small voltage vectors e.g. low voltage ride through in [8], while for high modulation indexes the situation will change due to more frequent application of the large voltage vectors. We can conclude that for solving this problem not only the hardware needs to be adapted but also the designed control algorithm needs to take into account different stress distributions in the operating points of the converter.

One of the most popular solutions was the active neutral point clamped (ANPC) topology, first introduced in [5]. By replacing the clamping diodes with the active switches, more redundant switching states can be achieved to balance out the loss distribution. Different commutations and zero states are used to distribute the losses more evenly. In [9] online calculations of the switching and conduction losses are used for the estimation of the junction temperatures, which are fed back to the control unit. In the next step, the applied switching state is selected from the decision chart for commutations to the zero states. Loss distributions of six PWM-based control strategies are compared in [10]. The proposed method has managed to outperform the other PWM modulation methods and balance out both the conduction and switching loss distribution, however the method was not experimentally validated in that paper. In [11] authors propose an adaptive double frequency PWM (ADF-PWM) that can adapt the duty cycles of every switching cycle to optimize the loss distribution. Nevertheless, it is not shown whether the algorithm also can balance the neutral point voltage or another control loop is necessary. Algorithms based on Finite-set model predictive control (FS-MPC) have the possibility to include multiple objectives in a single cost function without the necessity of additional control loops [12]–[14]. In [12] the FS-MPC is divided into two stages: in the first stage the cost function that includes the current control and DC-bus balance control is used and in the second a cost function that manages the loss energy balancing is used. Therefore, in the first stage 27 different voltage vectors are evaluated and in the second stage if the zero voltage vector is selected, predictions for 4 possible zero vectors are calculated. Both cost functions have two weighting factors, however it is not described how they should be optimally selected. The algorithm was modified in [13] where now only one cost function is used and the power losses are predicted using a function that contains the most stressed devices according to the switching transition. In this way the search time and the calculation time of the algorithm are reduced, though the weighting factor tuning still remained as the most difficult part of the control design. The control method presented in [14] Predictive Active Loss Balancing (PALB) is a combination of SHE-PWM and MPC. Despite the fact that the method showed decreased maximum junction temperature and increased output power, it was not

Table II: System parameter values.

Parameter	Value
DC-link voltage and capacitance (V_{dc} , $C_{dc1,2}$)	700 V, 2.8 mF
Filter inductance (L_f , C_f)	2.4 mH, 15 μ F
Load resistance (R_{load})	2.16 Ω
Sampling time (T_s)	20 μ s

offers a simple inclusion of multiple objectives in the control cost function and a fast transient response [22]. The objectives that need to be taken into account in the control design are: voltage reference tracking, neutral point balancing and device temperature balancing. As stressed in the previous sections, depending on the application (modulation index, power factor) the stress distribution of the ANPC converter will change. In our case, the converter is expected to be working with a high modulation index and unidirectional power flow. This means that the most stressed device will be the outer devices (S_1, S_4) [21]. Therefore, the algorithm needs to reduce the switching stress of these devices and distribute it to the inner SiC devices, which can operate on high switching frequencies with lower losses.

The schematic of the system can be seen in Fig. 2. In each sample period the FS-MPC controller collects the measurements of the DC-link voltages ($v_{dc1,2}$), converter output current (i_{fabc}), filter capacitor voltage ($v_{c,abc}$) and load current (i_{abc}) to calculate the propagations of the voltages for 27 possible switching states of the three phase converter. Using the Clark transformation the control variables are transformed from time domain components of the three phase abc system to the stationary $\alpha\beta$ reference frame. The propagations for the next sample period are calculated using the discretized system equations given in (1) - (3). Euler forward method is used to obtain the discrete system equations. Once the predictions are calculated, they are used in the cost function, which defines the desired behaviour of the converter.

$$v_{dc1,2}(t) = C_{dc1,2} \frac{di_{dc1,2}(t)}{dt} \quad (1)$$

$$i_{f\alpha\beta}(t) = C_f \frac{dv_{c\alpha\beta}(t)}{dt} + i_{o\alpha\beta}(t) \quad (2)$$

$$v_{i\alpha\beta}(t) = L_f \frac{di_{f\alpha\beta}(t)}{dt} + v_{c\alpha\beta}(t) \quad (3)$$

Three objectives will be used in the cost function (4): output voltage control, DC-link balancing and penalization for the switching of the outer switches i.e. favouring the switching of the inner switches $S_2 - S_3$:

$$g = (v_{c\alpha\beta}^* - v_{c\alpha\beta}^P)^2 + \lambda_{dc}g_{dc} + \lambda_pg_p \quad (4)$$

$$g_{dc} = (v_{dc1}^P - v_{dc2}^P)^2 \quad (5)$$

$$g_p = \sum_{x=a,b,c} (1 - |S_{2x}(k) - S_{2x}(k-1)|) + \quad (6)$$

$$(1 - |S_{3x}(k) - S_{3x}(k-1)|), \quad (7)$$

where weighting factors λ_{dc} and λ_p define the importance of each objective, $S_x(k-1)$ represents the previous and $S_x(k)$ the

current switching state for all converter phase legs $x \in a, b, c$. The optimum weighting factors can be determined by using the Artificial Neural Networks approach presented in [23].

IV. LOSS DISTRIBUTION AND DEVICE JUNCTION TEMPERATURE COMPARISON

A simulation model of the system presented in Fig. 2 and FS-MPC algorithm explained in the previous section were created in MATLAB Simulink. The thermal modeling of the devices was done in PLECS Blockset using the manufacturer datasheets. In Table II system parameters used for simulations to analyze the device stress under high power loading are presented. The weighting factors in the cost function (4) were set to $\lambda_{dc} = 5$ and $\lambda_p = 1$. A benchmark model using the carrier based algorithm based on phase disposition of the carriers presented in [17] was used for comparison. Due to the lack of modulator in the FS-MPC algorithm, the switching frequency of the converter is variable, therefore only the average switching frequency per device can be calculated using the following expression:

$$f_{swavg} = \sum_{i=1}^6 \frac{f_{swai} + f_{swbi} + f_{swci}}{3} \quad (8)$$

A. Simulation results

In Fig. 3 filter capacitor voltage and reference tracking error are shown. Even with the two secondary objectives in the cost function it can be noticed that the reference tracking of the algorithm has a good performance. The obtained simulation results of the loss distribution and device junction temperatures are shown in the Fig. 4. For the FS-MPC algorithm an average switching frequency of 14 kHz was calculated and for the benchmark model 15 kHz switching frequency was used. The total losses for the nominal output power of 73 kW for FS-MPC algorithm were 883 W ($\eta = 0.988$) and 1110 W ($\eta = 0.985$) for benchmark algorithm respectively. Although the overall efficiency was not significantly increased, lower losses per device can be noticed in the Fig. 4a. We can also notice that for the benchmark algorithm the only device producing the switching losses is the inner MOSFET and the total switching losses for FS-MPC algorithm are the same but they are spread over all devices. This difference can be explained by the fact that the switching sequence of the benchmark algorithm is fixed and it is always following the same pattern from Table I, whereas FS-MPC is evaluating in every sample step if it is possible to avoid switching the outer devices without significantly degrading the reference tracking performance and DC-link voltage balance. Moreover, it can be seen that the clamping switches are also being used more often than in the benchmark algorithm, but also the outer switches are producing lower conduction losses. All of this is mirrored into the junction temperatures of the devices, which are for the proposed algorithm lower. Lower and balanced device temperatures can increase both the lifetime of the converter and also the maximal power output.

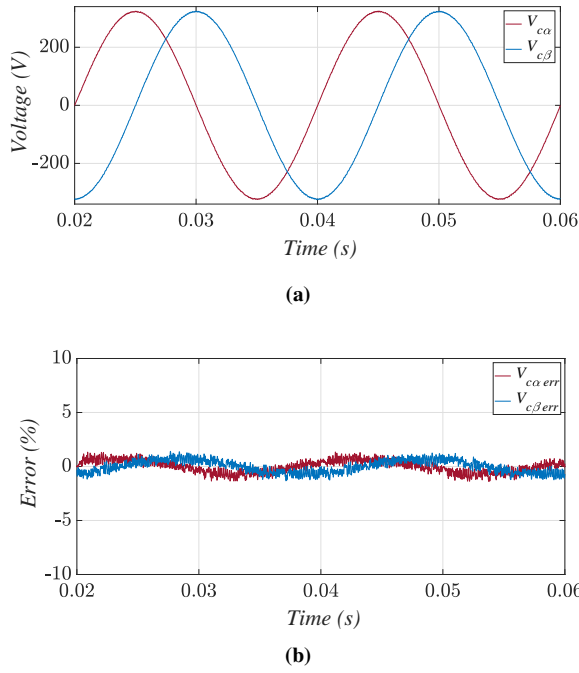


Fig. 3. Simulation results for the proposed FS-MPC algorithm: (a) capacitor voltage (b) voltage reference tracking error in $\alpha\beta$ reference frame.

It also needs to be noticed that the benchmark algorithm needs an additional control loop to maintain the DC-link balance, while in the FS-MPC algorithm this is already included in one control loop. This would have impact on the transients as the FS-MPC controller will have a faster response than in the benchmark model. The results are also compared to the loss distribution and junction temperatures of full Si ANPC module with MPC algorithm. In the loss distribution chart in Fig. 5a it can be seen that for the hybrid module the switching losses of the inner device and total losses on the outer device are lower. The positive effects are also visible in the thermal stress distribution given in Fig. 5b where the lower junction temperatures of the devices can be noticed.

B. Experimental results

In Fig. 6 the three phase prototype ANPC converter can be seen. The control algorithm is implemented using the MicroLabBox DS1202 PowerPC DualCore 2 GHz processor board and DS1302 I/O board from dSpace. The generated gate signals are then connected to the connector board from which the signals are guided through optic fiber cables to the converter board. To compensate the computational delay of the FS-MPC algorithm the predictions were calculated one step further ahead and applied at the beginning of the next time sampling interval as proposed in [22]. It was not possible to use the nominal current values in the experiments due to the set-up limitations (PCB design, DC-supply capacity, protection), therefore the testing was done for the $I_o = 30$ A and $V_{dc} = 260$ V.

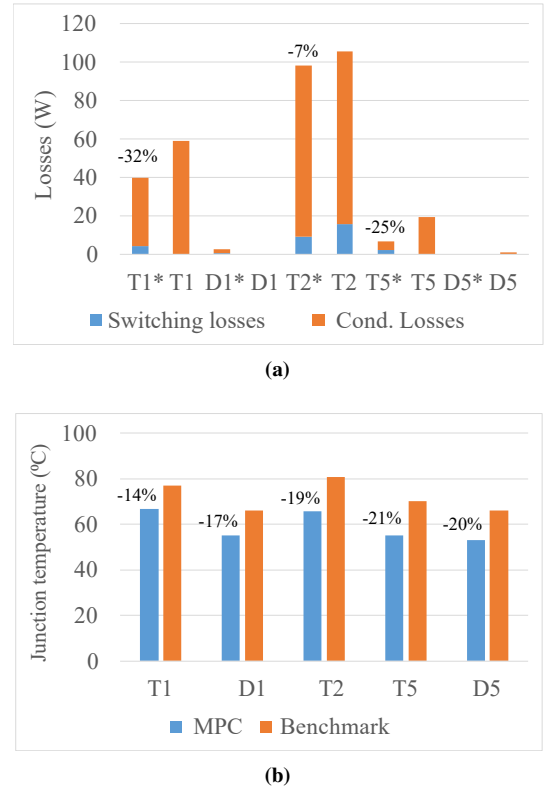
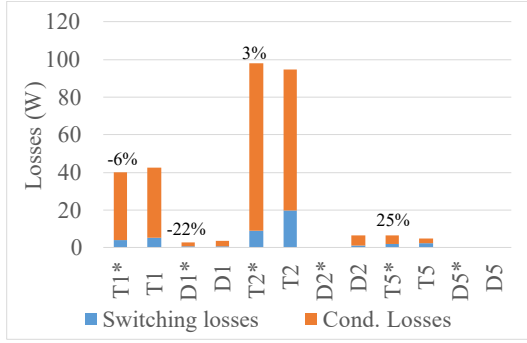


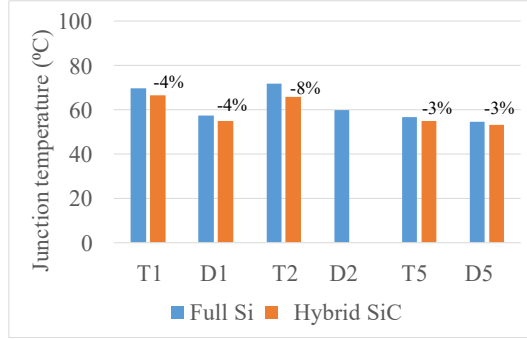
Fig. 4. Simulation results for one phase module: (a) device losses in a hybrid module for MPC (*) and benchmark algorithm. (b) device junction temperatures in a hybrid module MPC (*) and benchmark algorithm used in [17].

Measured phase load currents and DC-link voltages can be seen in Fig. 7. It can be noticed that the algorithm can keep a good balance of the DC-link voltages. An average switching frequency of 5.8 kHz was measured per device, the outer and clamping IGBT's (S_1, S_4, S_5, S_6) were switching with 1 kHz, while the MOSFET's (S_2, S_3) were switching with 15 kHz. For a comparison we will also show IR measurements of the conventional carrier based modulation with $f_{sw} = 5.8$ kHz and $f_{sw} = 15$ kHz. Here, it needs to be noticed that in this modulation scheme the outer and clamping IGBT's switch with 50 Hz and the MOSFET's with 5.8 kHz and 15 kHz respectively. Which of the two comparison metrics (average switching frequency per device or switching frequency of the MOSFET) should be used for a fair comparison opens up a lot of questions, therefore we will focus more on the temperature distribution rather than on the absolute values of the obtained temperatures.

In Fig. 8 a snapshot from the infrared camera can be seen for the proposed algorithm and the benchmark control algorithm. It can be seen that the temperatures of the upper device S_1 and inner device S_3 are very good balanced for all 3 control strategies. We can also notice that the distinction is found in the clamping device temperature as seen in Fig. 9. For the proposed algorithm the temperature difference of the clamping



(a)



(b)

Fig. 5. Simulation results for one phase module: (a) device losses for MPC in a hybrid ANPC module (*) and in full Si (b) device junction temperatures in a hybrid ANPC module (*) and in full Si.

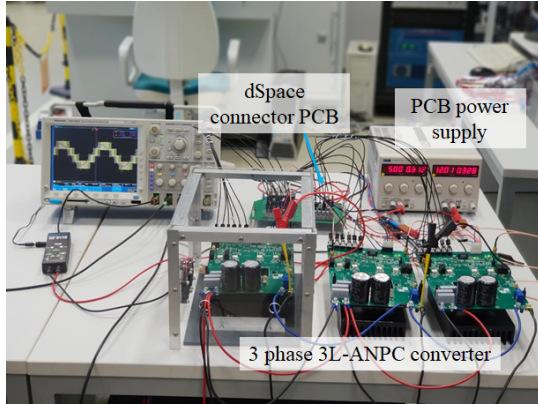
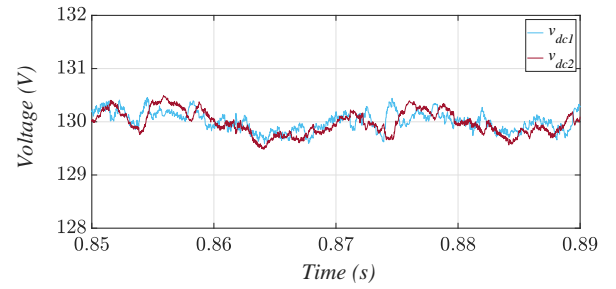


Fig. 6. Three phase ANPC experimental set-up

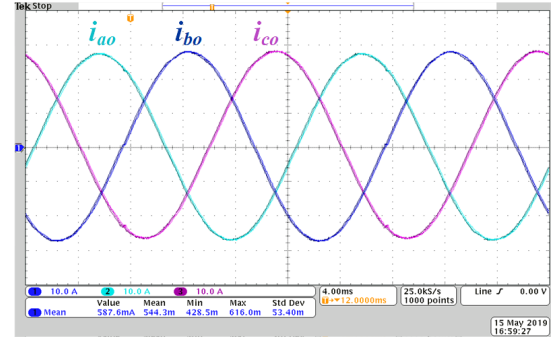
device and the outer device is 1.6°C , while for the benchmark model the difference is 3.8°C , see Table III. This result was expected as the proposed algorithm is switching the clamping device with a higher switching frequency providing better distribution of the losses among the devices.

V. CONCLUSION

A Finite Set Model Predictive Control algorithm is proposed to balance the temperatures in a hybrid ANPC module. This is achieved by penalization of the switching combinations that



(a)



(b)

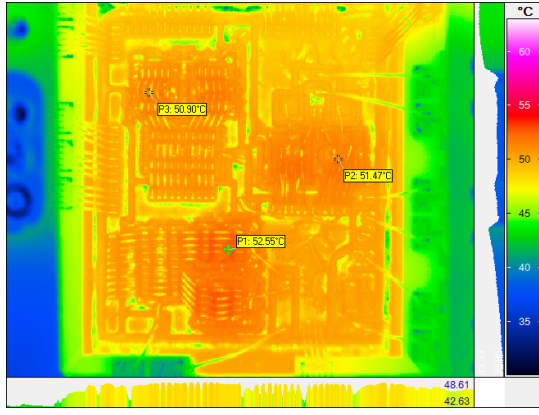
Fig. 7. Experimental measurements: (a) DC-link voltages $v_{dc1,2}$, (b) phase load currents i_{oabc} [10 A/div] at $P = 4$ kW.

Table III: Comparison of the measured junction temperatures for the three control strategies ($P = 4$ kW).

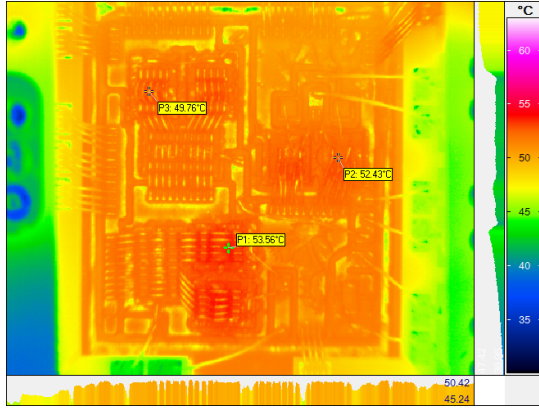
Control	Switching freq.	T_{j4}	T_{j4}	T_{j4}
FS-MPC	5.8 kHz	52.55°C	51.47°C	50.9°C
Bench. PWM	5.8 kHz	53.56°C	52.43°C	49.76°C
Bench. PWM	15 kHz	54.14°C	53.78°C	51.81°C

switch the outer switches more often in the cost function. As a consequence, the switching frequency of the inner switches will increase while in outer devices it will decrease. In this way the advantage of low switching losses of the SiC MOSFETs will be utilized. Simulation results for the nominal converter power showed that the proposed algorithm can provide balanced stress distribution and good reference tracking performance. This was also confirmed with experimental measurements which showed that the difference between the inner and outer device temperature is within 1°C . Moreover, it was showed that the proposed algorithm can maintain the DC-link voltages in good balance with voltage deviation below 0.5 V. An improvement compared to the conventional carrier based algorithm is also seen in the clamping device temperature which had a lower temperature difference to the outer device then when using the conventional algorithm.

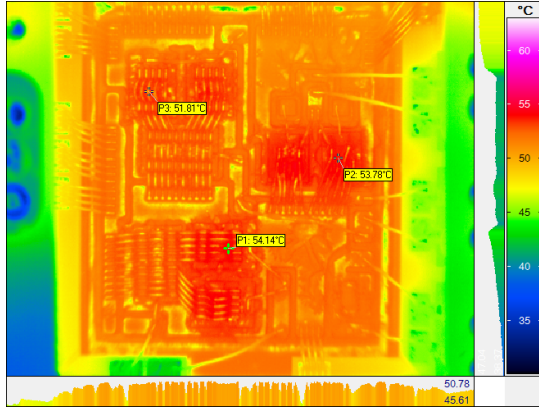
It this paper only a unidirectional power flow was investigated for e.g. photovoltaics application, in future work the thermal analysis of the hybrid ANPC converter using the



(a)



(b)



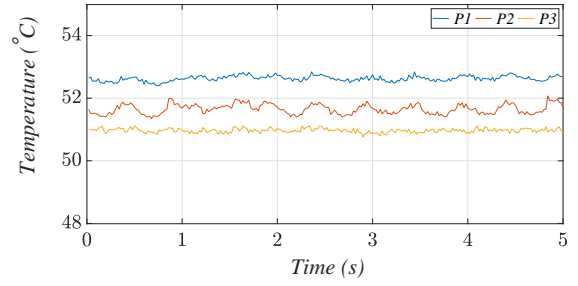
(c)

Fig. 8. IR snapshot of the one phase ANPC open module during operation, $V_{dc} = 260$ V, $I_o = 30$ A: (a) with the proposed FS-MPC algorithm, (b) with benchmark algorithm, $f_{sw} = 5.8$ kHz, (c) with benchmark algorithm, $f_{sw} = 15$ kHz.

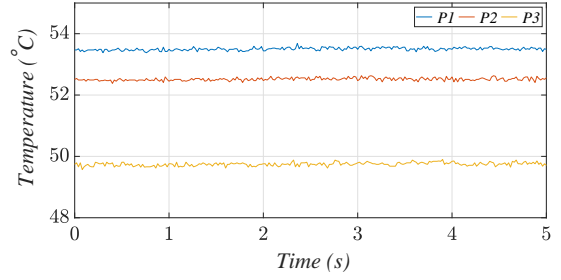
proposed algorithm will be extended for reverse power flow and low modulation indexes.

ACKNOWLEDGMENT

The authors would like to thank Danfoss Silicon Power GmbH for providing the hybrid SiC open modules that were used to evaluate the temperature distribution in this paper. This



(a)



(b)

Fig. 9. Junction temperature measurement for (P1 \rightarrow S4 (outer switch), P2 \rightarrow S3 (inner switch), P3 \rightarrow S6 (clamping switch)) in steady state, $V_{dc} = 260$ V, $I_o = 30$ A: (a) with proposed FS-MPC algorithm, (b) with benchmark algorithm, $f_{sw} = 5.8$ kHz (see Fig. 8).

work was supported in part by the European Research Council (ERC) under the European Unions Seventh Framework Program (FP/2007-2013)/ERC Grant 616344 - HEART, and in part by the Federal Ministry for Economic Affairs and Energy Program (0325797A) - Entwicklung, Bau und Betrieb eines Mittelfrequenz-Mittelspannungs-Messstrom-Erzeugers für Netzmessungen und Optimierungen.

REFERENCES

- [1] A. Nabae, I. Takahashi, and H. Akagi, "A new neutral-point-clamped PWM inverter," *IEEE Trans. Ind. Appl.*, vol. 17, no. 5, pp. 518–523, Sept 1981.
- [2] Y. Wang and F. Wang, "Novel three-phase three-level-stacked neutral point clamped grid-tied solar inverter with a split phase controller," *IEEE Trans. Power Electron.*, vol. 28, no. 6, pp. 2856–2866, June 2013.
- [3] E. J. Bueno, S. Cobrecas, F. J. Rodriguez, . Hernandez, and F. Espinosa, "Design of a back-to-back NPC converter interface for wind turbines with squirrel-cage induction generator," *IEEE Trans. Energy Conversion*, vol. 23, no. 3, pp. 932–945, Sep. 2008.
- [4] H. R. Teymour, D. Sutanto, K. M. Muttaqi, and P. Ciufo, "Solar PV and battery storage integration using a new configuration of a three-level NPC inverter with advanced control strategy," *IEEE Trans. Energy Conversion*, vol. 29, no. 2, pp. 354–365, June 2014.
- [5] T. Bruckner and S. Bemet, "Loss balancing in three-level voltage source inverters applying active NPC switches," in *Proc. IEEE 32nd Annual Power Electron. Specialists Conf.*, vol. 2, 2001, pp. 1135–1140 vol.2.
- [6] J. Rodriguez, S. Bernet, P. K. Steimer, and I. E. Lizama, "A survey on neutral-point-clamped inverters," *IEEE Trans. Ind. Electron.*, vol. 57, no. 7, pp. 2219–2230, July 2010.
- [7] U. M. Choi and F. Blaabjerg, "Asymmetric power device rating selection for even temperature distribution in NPC inverter," in *Proc. IEEE Energy Conversion Congress and Exposition (ECCE)*, Oct 2017, pp. 4196–4201.

- [8] K. Ma and F. Blaabjerg, "Modulation methods for neutral-point-clamped wind power converter achieving loss and thermal redistribution under low-voltage ride-through," *IEEE Trans. Ind. Electron.*, vol. 61, no. 2, pp. 835–845, Feb 2014.
- [9] T. Bruckner, S. Bernet, and H. Guldner, "The active NPC converter and its loss-balancing control," *IEEE Trans. Ind. Electron.*, vol. 52, no. 3, pp. 855–868, June 2005.
- [10] G. Zhang, Y. Yang, F. Iannuzzo, K. Li, F. Blaabjerg, and H. Xu, "Loss distribution analysis of three-level active neutral-point-clamped (3L-ANPC) converter with different PWM strategies," in *2016 IEEE 2nd Annual Southern Power Electronics Conference (SPEC)*, Dec 2016, pp. 1–6.
- [11] Y. Deng, J. Li, K. H. Shin, T. Viitanen, M. Saeedifard, and R. G. Harley, "Improved modulation scheme for loss balancing of three-level active NPC converters," *IEEE Trans. on Power Electron.*, vol. 32, no. 4, pp. 2521–2532, April 2017.
- [12] D. Andler, M. Perez, J. Rodríguez, and S. Bernée, "Predictive control of three-level active NPC converter with evenly energy losses distribution," in *The 2010 International Power Electronics Conference (ECCE ASIA)*, June 2010, pp. 754–759.
- [13] D. Andler, J. Weber, S. Bernet, and J. Rodríguez, "Improved model predictive control with loss energy awareness of a 3L-ANPC voltage source converter," in *2010 International Conference on Applied Electronics*, Sept 2010, pp. 1–6.
- [14] D. Andler, E. Hauk, R. Álvarez, J. Weber, S. Bernet, and J. Rodríguez, "New junction temperature balancing method for a three level active NPC converter," in *Proceedings of the 2011 14th European Conference on Power Electronics and Applications (EPE)*, Aug 2011, pp. 1–9.
- [15] M. Schweizer, T. Friedli, and J. W. Kolar, "Comparison and implementation of a 3-level NPC voltage link back-to-back converter with SiC and Si diodes," in *2010 Twenty-Fifth Annual IEEE Applied Power Electronics Conference and Exposition (APEC)*, Feb 2010, pp. 1527–1533.
- [16] D. Zhang, J. He, and D. Pan, "A megawatt-scale medium-voltage high efficiency high power density "SiC+Si" hybrid three-level ANPC inverter for aircraft hybrid-electric propulsion systems," in *2018 IEEE Energy Conversion Congress and Exposition (ECCE)*, Sept 2018, pp. 806–813.
- [17] Q. Guan, C. Li, Y. Zhang, S. Wang, D. D. Xu, W. Li, and H. Ma, "An extremely high efficient three-level active neutral-point-clamped converter comprising SiC and Si hybrid power stages," *IEEE Trans. Power Electron.*, vol. 33, no. 10, pp. 8341–8352, Oct 2018.
- [18] S. Vazquez, J. I. Leon, L. G. Franquelo, J. Rodriguez, H. A. Young, A. Marquez, and P. Zanchetta, "Model predictive control: A review of its applications in power electronics," *IEEE Ind. Electron. Magazine*, vol. 8, no. 1, pp. 16–31, March 2014.
- [19] S. Vazquez, J. Rodriguez, M. Rivera, L. G. Franquelo, and M. Norambuena, "Model predictive control for power converters and drives: Advances and trends," *IEEE Trans. Ind. Electron.*, vol. 64, no. 2, pp. 935–947, Feb 2017.
- [20] T. Dragicevic, "Model predictive control of power converters for robust and fast operation of AC microgrids," *IEEE Trans. Power Electron.*, vol. 33, no. 7, pp. 6304–6317, July 2018.
- [21] M. Novak, V. Šunde, N. Čobanov, and Z. Jakopović, "Semiconductor loss distribution evaluation for three level ANPC converter using different modulation strategies," in *2017 19th International Conference on Electrical Drives and Power Electronics (EDPE)*, Oct 2017, pp. 170–177.
- [22] J. Rodriguez and P. Cortes, *Predictive Control of Power Converters and Electrical Drives*, ser. Wiley - IEEE. Wiley, 2012.
- [23] T. Dragicevic and M. Novak, "Weighting factor design in model predictive control of power electronic converters: An artificial neural network approach," *IEEE Trans. Ind. Electron.*, pp. 1–12, Early Access.